Nonlinear Focusing in Dynamic Crack Fronts and the Microbranching Transition

Itamar Kolvin,[1] Jay Fineberg,[1] and Mokhtar Adda-Bedia[2]
[1]Racah Institute of Physics, The Hebrew University of Jerusalem, Jerusalem, Israel 9190401
[2]Université Lyon, Ecole Normale Supérieure de Lyon, Université Claude Bernard, CNRS, Laboratoire de Physique, F-69342 Lyon, France
(Received 10 August 2017; published 21 November 2017)

Cracks in brittle materials produce two types of generic surface structures: facets at low velocities and microbranches at higher ones. Here we observe a transition from faceting to microbranching in polyacrylamide gels that is characterized by nonlinear dynamic localization of crack fronts. To better understand this process we derive a first-principles nonlinear equation of motion for crack fronts in the context of scalar elasticity. Its solution shows that nonlinear focusing coupled to rate dependence of dissipation governs the transition to microbranching.

DOI: 10.1103/PhysRevLett.119.215505

Fracture is typically an irregular process [1–13]. Cracks show a strong tendency for instability creating nonsmooth surfaces with rich structure. Crack instabilities and their associated structure exhibit a strong dependence on crack velocity: slow tensile cracks ($v \ll c_R$, where c_R is the Rayleigh wave speed) are prone to nucleate steps which drift along the crack front and divide the fracture surface into facets [2–6]; faster tensile cracks may be unstable to both void nucleation [8] and the formation of microbranches—microscopic cracks that branch off the main crack front [9–13]. Linear perturbation theory, however, predicts that *any* initial disturbance to a tensile crack front should either decay as the crack progresses [14–16] or disperse as outgoing waves [17,18]. Current linear theories are therefore incapable of reproducing the observed fracture surfaces.

In recent nonperturbative approaches to fracture, such as lattice models [19,20] and phase-field models [21,22], localized crack branching arises naturally, regardless of the specific dissipative process. Both approaches predict that microbranching is governed by the microscopic dissipation length scale and that instability initiates at $v_c \sim 0.7c_R$. This critical velocity is significantly higher than that observed in experiments, and predicted from energy considerations in the theory of 2D branching [23,24]. In addition, microbranch dimensions typically exceed the process zone size by a few orders of magnitude. It therefore remains unclear what component or mechanism is missing in the existing models.

In polyacrylamide gels, cracks exhibit a transition between facet formation and microbranching at $v \sim 0.05$–$0.1c_R$ [6]. The transition is not sharp, and both types of structures may coexist in the transition region. A typical fracture surface (for $v \sim 0.06c_R$) shown in Fig. 1(a) features both microbranches and facets. Shadow imaging of the fracture plane reveals the in-plane projection of the crack front dynamics during the formation of these structures, as depicted in Fig. 1(b): in the upper right part of the panel, a facet forms by a pair of steadily diverging steps. Each step induces a cusplike deformation of the *in-plane* crack front. In the lower left part of the panel, a microbranch similarly initiates as a pair of diverging steps, that gradually change their direction and converge. Although the global conditions were identical, the two structures did not meet the same fate. How does the crack "decide" which structure will eventually form? A close inspection reveals that microbranch formation involves stronger front curvatures than facet formation. Hence, microbranches embody stronger perturbations to the crack front.

While crack fronts execute both in-plane and out-of-plane motions, we will study the response of a simplified

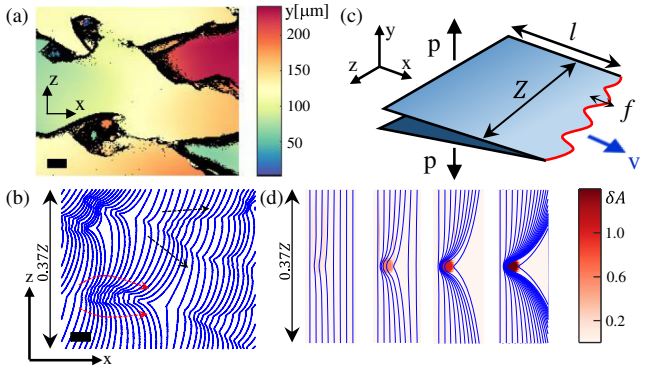

FIG. 1. Experimental fracture surface (a) formed by tensile crack fronts (b) moving at $\sim 0.06c_R$ and displayed at 0.13 ms intervals. The surface features both facets (upper and lower right) and microbranches (upper and lower left). A pair of step lines nucleate and diverge forming a facet (black arrows) while a microbranching event ends with cusp formation (red arrows). The black scale bars are 200 μm long. (c) Geometry of the model. Two line loads p moving with a speed v are driving a planar crack front at a distance l. The crack front is perturbed around a straight configuration with amplitude $f(z,t)$. (d) Crack fronts, calculated via Eq. (1), move at velocity $v = 0.05c$ and encounter obstacles with increasing toughness; see text following Eq. (3) for details. Fronts are plotted at the same time intervals as in (b) when identifying $c = c_R$.

in-plane model to externally induced perturbations. This model retains all of the essential features of the full elastodynamic problem [25]. As the transition to microbranching apparently depends on the amplitude of the perturbation, we must consider nonlinear perturbations to dynamic crack fronts. In this framework, we derive and solve an equation of motion for planar crack fronts that is exact to the 2nd order in front perturbation. In a homogeneous and isotropic medium, crack front motion is dictated by specifying the local normal velocity $v_\perp$ [26]. Cracks propagate when the energy flow into the crack per unit area, G or energy release rate, is balanced by the dissipation Γ involved in creating the two new fracture surfaces. Energy flow into the crack tip is regulated by a universal function $g(v_\perp)$, which approaches 1 when $v_\perp \to 0$ and 0 when $v_\perp \to c_R$ [27]. Consider a straight crack front confined to the xz plane and propagating along the x axis with velocity v. When the front is perturbed, i.e., its position is given by $x = vt + f(z,t)$ [see Fig. 1(c)], local energy balance $G = \Gamma$ reads

$$G_0 g(v_\perp)(1 + H[f]) = \Gamma(x, z; v_\perp), \tag{1}$$

where G_0 is the energy release rate of the unperturbed crack. The perturbation f introduces a term $H[f]$ which depends on the history of the crack front, and can be computed order by order in f, through a solution of the elastodynamic problem [17,28–30]. The fracture energy Γ may vary locally along the front and depend on crack velocity [31,32].

Computing G requires an asymptotic solution of the 3D vector displacement field in the vicinity of the crack front. For a tensile (mode I) crack, G is given by the J integral involving the product of stress and displacement rate [27]. A calculation results in the expression $G = PK$, where $K = \sqrt{2\pi}\lim_{X\to 0^+}\sigma_{yy}(x,0,z)X^{1/2}$ and $P = \lim_{X\to 0^-} u_y(x,0,z)(-X)^{-1/2}$ are the stress and displacement intensity factors, respectively [30]. Here σ_{ij} denotes the stress tensor, u_i is the displacement vector, and $X = x - vt - f$. The mode I elastodynamic problem consists of simultaneously solving three decoupled scalar wave equations, with wave velocities being the longitudinal and the shear wave speeds, respectively. Free boundary conditions on the crack faces, however, mix the wave polarizations, rendering the problem quite formidable. Nonlinear corrections to G have not been explicitly computed yet in the general dynamic case [29,33].

Fortunately, G can also be derived in a simpler analogous model which involves only a single scalar field ϕ satisfying a wave equation with wave speed c [25,34]. In the quasistatic limit, the elastic fields in the bulk can be exactly written in terms of the scalar potential ϕ [35], and on the $y = 0$ boundary one obtains the simple forms $u_y = \phi$ and $\sigma_{yy} = \partial_y \phi$. Moreover, both the scalar model and mode I elastodynamics contain wavelike modes that maintain front coherence, and the universal function in the scalar model, $g(v) = \sqrt{(1 - v/c)/(1 + v/c)}$, closely resembles that of the mode I fracture [36]. In the following, we set $c = 1$ for convenience.

Our derivation of G uses a matched asymptotic expansion (MAE) approach [30]. Here we present only a sketch of the derivation, which will be provided in detail elsewhere [37]. Figure 1(c) depicts a crack front driven by two line loads p located at a distance l from the crack front and moving at a constant velocity v. In the absence of perturbations, the loads p cause the crack front to propagate steadily at a velocity v. Since our problem is symmetric with respect to the $y = 0$ plane, the scalar field ϕ can be determined by solving the wave equation in the $y > 0$ half-space with zero displacement $\phi|_{y=0} = 0$ for $X > 0$ and zero stress $\partial_y \phi|_{y=0} = 0$ for $X < 0$.

The MAE consists of matching solutions at two scales of the problem. Assuming that $f \ll l$, we first find an "inner" solution for ϕ in the vicinity of the crack front written as an expansion in powers of X and of f. The inner solution contains integration constants that should be determined by matching to an "outer" solution dominated by the length scale of the system l. In the inner solution, the most singular power must be $\phi \sim X^{1/2}$ since it ensures a finite G. Far from the crack front, however, the expansion $X^{1/2} \simeq \sqrt{x - vt} - \frac{1}{2}(f/\sqrt{x - vt}) - \frac{1}{8}[(f^2)/(x - vt)^{3/2}] + \cdots$ only appears to create stronger "unphysical" singularities at the location of the unperturbed front $x = vt$. The outer solution, which can be found independently of f, is expanded in powers of $x - vt$ and the coefficients obtained from both solutions are then compared. For each order of the perturbation only a finite number of coefficients needs to be matched. By this method, the intensity factors P and K are obtained from the coefficient of the $X^{1/2}$ component of the field ϕ.

The main result of our calculation is an expression for the history functional $H[f]$ up to second order in f. First, we define the linear functionals in Fourier space $\hat{\Psi}[\hat{f}] = \alpha k \int_{-\infty}^{t} dt' J_1[\alpha k(t - t')]\hat{f}(k, t')/(t - t')$ and $\hat{\Psi}_2[\hat{f}] = \alpha^2 k^2 \int_{-\infty}^{t} dt' J_2[\alpha k(t - t')]\hat{f}(k, t')/(t - t')$, where $\alpha = \sqrt{1 - v^2}$, J_1 (J_2) is the 1st (2nd) order Bessel functions and the hats denote the spatial Fourier transform, i.e., $\hat{f}(k,t) = \int dz e^{-ikz} f(z,t)$. With these definitions the history functional is given in real space by

$$H[f] = -\frac{1}{\alpha^2}\Psi[f] + \frac{1}{4\alpha^4}\Psi[f]^2 + \frac{1}{2\alpha^4}\Psi[f\Psi[f]] - \frac{1 - 2v}{4\alpha^4}\Psi_2[f^2] - \frac{1 + 2v}{2\alpha^4} f\Psi_2[f]. \tag{2}$$

In this expression we neglected terms of order $O(f/l)$, and consequently $H[f]$ becomes invariant to translation $f \to f + C$, where C is a constant. Taking f to be time independent and $v \to 0$, Eq. (2) recovers the corrections to G calculated for quasistatic crack fronts [38]. On the other hand, assuming that f does not depend on z, the history

functional is identically zero, and Eq. (1) becomes the 2D equation of motion given in Ref. [25].

Equation (1) neatly links local dissipation involved in the creation of new surfaces with the elastodynamic response of the crack front. In experiment, the cost for creating a unit surface area may be rate dependent and the formation of surface and subsurface structure locally increases dissipation. Here we mimic the experimental situation by expressing the fracture energy as a product of two parts,

$$\Gamma(x,z;v_\perp)=\Gamma_0(v_\perp)[1+\delta A(x,z)], \tag{3}$$

where the "bare" fracture energy $\Gamma_0(v)=\tilde{\Gamma}_0(1+av)$ grows linearly with crack velocity and δA quantifies the local relative increase in dissipation.

We now test how crack fronts respond dynamically to perturbations. Expanding all quantities in Eq. (1) to the 2nd order in f we obtain a nonlinear equation of motion for the crack front [39]. The explicit equation of motion contains a geometric term $\frac{1}{2}vf_z^2$ which accounts for propagation along the local normal to the front, elastic terms that stem from $H[f]$, and dissipative terms that depend on δA. We may now numerically propagate the crack front using an Euler scheme under periodic boundary conditions along an interval of length Z [see Fig. 1(c)].

We first test the crack front response to a disk-shaped obstacle. δA is taken to be constant inside the obstacle, while decaying smoothly and rapidly to zero outside. To minimize system size effects we take the diameter of the obstacle to be $d=0.025Z$. Figure 1(d) shows crack fronts moving at $v=0.05$ and encountering obstacles with increasing toughness. The fronts were discretized over $N=512$ mesh points. As in the polyacrylamide gels used in our experiment, we assumed that the fracture energy grows linearly with velocity with $a=4$. As the obstacle toughness increases, the crack front dynamically develops increasingly higher curvatures while detaching from the obstacle. During detachment the elastic tension stored in the front is released, driving the crack front to accelerate to high velocities. Increasing mesh resolution did not affect the peak curvature, indicating that elasticity arrests further curvature growth.

Surprisingly, crack front dynamics are *defocusing* when the fracture energy is velocity independent (i.e., $a=0$). Figure 2 compares curvature evolution for $a=0$ and $a=4$ at $v=0.3$ and $\delta A=1.2$. When $a=4$, the front locally decelerates as it enters the obstacle and curvature builds up continuously, first gradually and then rapidly as it breaks free. Comparison with the solution using only 1st order terms shows that the nonlinearities produce curvatures up to $\sim 6\kappa_{\rm disk}=12/d$, while front curvature remains $\sim\kappa_{\rm disk}$ when suppressing nonlinearity. For $a=0$, the velocity-independent case, the front curvature quickly reaches a plateau at $\sim\kappa_{\rm disk}/2$, while a 1st order solution under the same conditions develops higher curvatures.

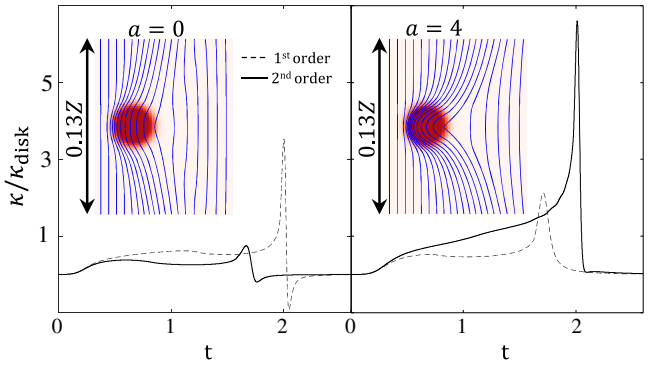

FIG. 2. Change of front dynamics from defocusing to focusing when increasing $a=(d\log\Gamma_0/dv)|_{v=0}$. Panels show curvature evolution at the obstacle midline for velocity-independent fracture energy (left) and for velocity-dependent fracture energy (right). Here $v=0.3$, $\delta A=1.2$ and $\kappa_{\rm disk}=2/d=80/Z$. The 1st order solution is drawn for comparison (dashed line). Insets depict crack front profiles drawn over the spatial fracture energy distribution.

The transition from crack front defocusing to self-focusing with increasing a is a generic property of the nonlinear equation of motion. Equation (1) can be solved analytically in the case of a time-independent cosine perturbation $\delta A=D\cos(z)$. The resulting front shape is $f(z)=-\alpha D\cos(z)+D^2v_2t+D^2f_2\cos(2z)$ where v_2 and f_2 are rational functions of a and v [39]. The point of maximum curvature is $z=0$ and there $f''(z=0)=\alpha D-4D^2f_2$, so the front is focusing when $f_2<0$ and defocusing otherwise. Analysis shows that f_2 becomes negative when the dimensionless parameter $\sqrt{1-v^2}d\log\Gamma_0/dv=a\sqrt{1-v^2}/(1+av)\gtrsim 1$. Thus, front curvature grows sublinearly with D when $\sqrt{1-v^2}d\log\Gamma_0/dv\lesssim 1$ and superlinearly otherwise. An extensive study of the (a,v) parameter plane for the encounter of a front with a disk-shaped obstacle yielded the same trends [39].

Can the nonlinear self-focusing seen here drive the transition from facet to microbranch formation? As seen in Fig. 1(b), both structures are composed of step lines that in one case diverge and in the other converge. To answer this question we use the results of our experimental studies of facet formation [6], which showed that the formation of a step incurs a local energetic cost of $\Gamma_0\delta A(z-z_0)$. Here z_0 is the position of the step along the front and $\delta A=(D/\pi)[1\pm\alpha(z/w)]/[1+(z/w)^2]$, where $\alpha=0.24$. During crack propagation steps drift and grow, leading to changes in position z_0 and width w. The width is assumed to be much smaller than system dimensions $w\ll Z$, so that $\delta A(z)$ is a sharply peaked distribution. Locally, a step-line forms a constant $\sim 45°$ angle with the front slope [6]. To numerically propagate the distribution δA we draw a 45° line from z_0 at a given time step and its intersection with the front at the next time step determines the new value of z_0.

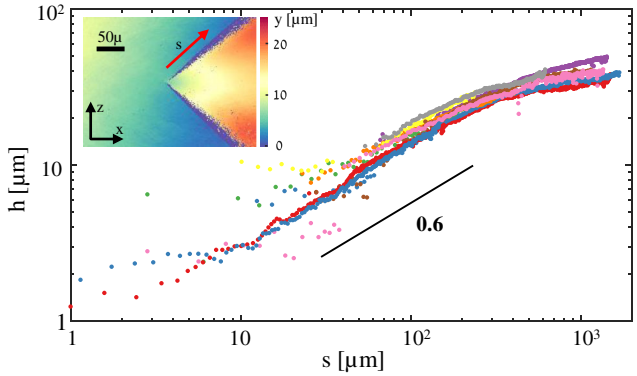

FIG. 3. The growth of step height along the step-line backbone s taken from pair nucleation events. Data are shown from nine step lines taken from five events. For two of the step lines (red and blue points), we performed a high resolution measurement (at 0.5 μm/pix). (inset) The high resolution surface scan.

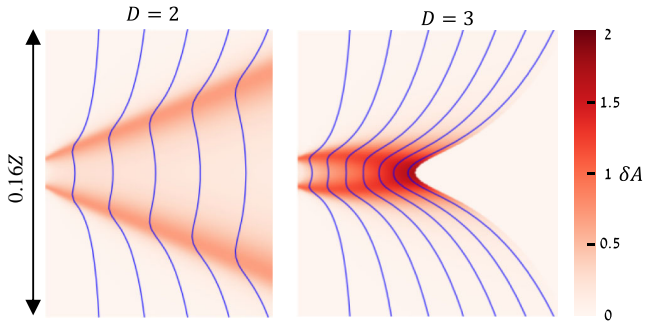

FIG. 4. Transition from step-line divergence (left) to step-line convergence (right) when increasing the dissipation amplitude D. Here $v = 0.1$, $a = 4$, and $\xi = 0.0016Z$. This is the same qualitative behavior as observed experimentally in Fig. 1(b). See movies in the Supplemental Material [39].

Lastly, we need to specify how steps grow with crack propagation. To this end, we consider the measured growth of step height h obtained by profilometry on surfaces formed by the tensile fracture of polyacrylamide gel (for details, see Ref. [6]). While step growth is highly sensitive to the presence of neighboring step lines and sample boundaries, we find that steps nucleating in pairs at a sufficient distance from other structures follow a reproducible trend, as shown in Fig. 3. Step heights grow along the step-line backbone s as $h/\xi \sim (s/\xi)^b$ with $b = 0.6 \pm 0.1$ and $\xi = 2 \pm 1$ μm. Assuming that step widths and heights grow in proportion to each other, we take $w = [\xi(x + \xi)]^{0.5}$ where x is the position of the front at time t and $z = z_0$; the distribution δA has a width $w = \xi$ at $t = 0$.

We numerically solve Eq. (1) for two initially diverging step lines with the parameters $v = 0.1, a = 4, \xi = 0.0016Z$. Step-line centers were initially separated by 10ξ and the front was straight.

The left panel of Fig. 4 depicts crack front and local fracture energy evolution for an amplitude of $D = 2$. The two step lines diverge with an angle that continually increases during propagation. Increasing the amplitude of δA to $D = 3$ causes the step lines to converge instead of diverging (see the right panel of Fig. 4). In our previous study [6] we have seen that $\int dz \delta A \sim 1.4h$. For $w \sim h/2$, this relation translates into $D \sim 2.8$. This suggests that convergence in the simulation may occur within the same parameter range as observed experimentally.

Additional simulations show similar trends; decreasing a and increasing v pushes the transition to step-line convergence to higher values of D. Changing ξ, however, does not affect the transition, but only the overall scale of the process. When solving Eq. (1) under the same conditions as Fig. 4, but neglecting 2nd order terms, no convergence was observed.

How general is the nonlinear focusing observed here? The crack front equation of motion presented here was derived in the context of a scalar approximation to elasticity and based on the assumption of planarity. We believe, however, that our results are not constrained by these assumptions. Perturbations of the crack front in both scalar and vector models generically decay. When $a = 0$, the wavelike modes that transmit stress along the crack front decay as $1/\sqrt{t}$ in the scalar model following an encounter with an asperity; in mode I elastodynamics, wave amplitudes undergo a short decay phase followed by a fixed value ("front waves") [36]. However, for $a > 0$ these modes decay exponentially in both theories. Moreover, the dimensionless parameter $\sqrt{1 - v^2} d \log \Gamma_0 / dv$ will arise in any nonlinear treatment of crack front perturbations, independent of the model used. Planarity, on the other hand, coupled with locally increased dissipation appears to be a good approximation to the in-plane shape of crack fronts forming surface structures, as was shown in Ref. [6]. This observation relies on the increase in dissipation due to the additional surface area formed by the crack. However, considering the full 3D dynamics is crucial for any theory attempting to capture step growth, drift, and step intersections.

What are the implications of our results to the microbranching instability? Microbranching is a complex phenomenon, and some of its features are material dependent. Our findings suggest that microbranch localization in z results from the development of high in-plane curvature along the crack front. Our model predicts how local curvature is controlled by three parameters: the local dissipation δA, the crack velocity v, and $(d \log \Gamma_0 / dv) = a/(1 + av)$. In the linear limit $\delta A \ll 1$; δA increases curvature while v diminishes it. When $\delta A \sim 1$ nonlinear effects become important. For $\sqrt{1 - v^2} d \log \Gamma_0 / dv \leq 1$ curvature increase with dissipation is sublinear while for $\sqrt{1 - v^2} d \log \Gamma_0 / dv \geq 1$ it is superlinear. In experiments, δA and v are not independent; as v increases, surface and subsurface structure becomes more complex leading to dynamically increased dissipation with v. This effective

increase in δA may be significant, possibly explaining why experiments [6,10] indicate that faster cracks are more susceptible to out-of-plane perturbations.

A previously unappreciated dimensionless parameter, $\sqrt{1-v^2}d\log\Gamma_0/dv$, that controls the sign and magnitude of nonlinear focusing, may explain at least part of the variation in microbranching between materials. For example, self-focusing might be the reason why in polyacrylamide gels, where $a \sim 3.3$, microbranches appear at $v \sim 0.1c_R$, and in soda-lime glass, where $a \sim 0$, microbranches appear at $v \sim 0.4c_R$. Further study of crack front dynamics in the presence of nonlinear elasticity [40,41] as well of the nucleation and growth of surface structure is needed to clarify our understanding of the microbranching transition.

We thank Eran Bouchbinder for a thorough reading of the manuscript. J. F. and I. K. acknowledge the support of the Israel Science Foundation (Grant No. 1523/15), as well as the US-Israel Bi-national Science Foundation (Grant No. 2016950).

[1] J. Schmittbuhl and K. J. Måløy, Phys. Rev. Lett. **78**, 3888 (1997).
[2] J. R. Kermode, T. Albaret, D. Sherman, N. Bernstein, P. Gumbsch, M. C. Payne, G. Csányi, and A. De Vita, Nature (London) **455**, 1224 (2008).
[3] T. Baumberger, C. Caroli, D. Martina, and O. Ronsin, Phys. Rev. Lett. **100**, 178303 (2008).
[4] Y. Tanaka, K. Fukao, Y. Miyamoto, and K. Sekimoto, Europhys. Lett. **43**, 664 (1998).
[5] A. Gent and C. Pulford, J. Mater. Sci. **19**, 3612 (1984).
[6] I. Kolvin, G. Cohen, and J. Fineberg, Nat. Mater., DOI: 10.1038/nmat5008 (2017).
[7] D. Bonamy, S. Santucci, and L. Ponson, Phys. Rev. Lett. **101**, 045501 (2008).
[8] J. Scheibert, C. Guerra, F. Célarié, D. Dalmas, and D. Bonamy, Phys. Rev. Lett. **104**, 045501 (2010).
[9] J. Fineberg and E. Bouchbinder, Int. J. Fract. **196**, 33 (2015).
[10] T. G. Boué, G. Cohen, and J. Fineberg, Phys. Rev. Lett. **114**, 054301 (2015).
[11] A. Livne, G. Cohen, and J. Fineberg, Phys. Rev. Lett. **94**, 224301 (2005).
[12] E. Sharon and J. Fineberg, Phys. Rev. B **54**, 7128 (1996).
[13] I. Kolvin, G. Cohen, and J. Fineberg, Phys. Rev. Lett. **114**, 175501 (2015).
[14] H. Gao and J. R. Rice, J. Appl. Mech. **56**, 828 (1989).
[15] R. Ball and H. Larralde, Int. J. Fract. **71**, 365 (1995).
[16] S. Ramanathan, D. Ertaş, and D. S. Fisher, Phys. Rev. Lett. **79**, 873 (1997).
[17] S. Ramanathan and D. S. Fisher, Phys. Rev. Lett. **79**, 877 (1997).
[18] M. Adda-Bedia, R. E. Arias, E. Bouchbinder, and E. Katzav, Phys. Rev. Lett. **110**, 014302 (2013).
[19] S. I. Heizler and D. A. Kessler, Phys. Rev. E **92**, 012403 (2015).
[20] S. I. Heizler and D. A. Kessler, Phys. Rev. E **95**, 063004 (2017).
[21] H. Henry and M. Adda-Bedia, Phys. Rev. E **88**, 060401 (2013).
[22] J. Bleyer and J.-F. Molinari, Appl. Phys. Lett. **110**, 151903 (2017).
[23] J. Eshelby, in *Fundamental Contributions to the Continuum Theory of Evolving Phase Interfaces in Solids* (Springer, New York, 1999), pp. 82–119.
[24] E. Katzav, M. Adda-Bedia, and R. Arias, Int. J. Fract. **143**, 245 (2007).
[25] J. R. Rice, Y. Ben-Zion, and K.-S. Kim, J. Mech. Phys. Solids **42**, 813 (1994).
[26] J. A. Hodgdon and J. P. Sethna, Phys. Rev. B **47**, 4831 (1993).
[27] L. B. Freund, *Dynamic Fracture Mechanics* (Cambridge University Press, Cambridge, England; New York, 1990).
[28] J. Willis and A. Movchan, J. Mech. Phys. Solids **43**, 319 (1995).
[29] J. Willis, Int. J. Fract. **184**, 17 (2013).
[30] A. N. Norris and I. D. Abrahams, J. Eng. Math. **59**, 399 (2007).
[31] E. Bouchbinder, J. Fineberg, and M. Marder, Annu. Rev. Condens. Matter Phys. **1**, 371 (2010).
[32] T. G. Boué, R. Harpaz, J. Fineberg, and E. Bouchbinder, Soft Matter **11**, 3812 (2015).
[33] J. R. Willis and N. V. Movchan, Math. Mech. Solids **19**, 82 (2014).
[34] G. Perrin and J. R. Rice, J. Mech. Phys. Solids **42**, 1047 (1994).
[35] M. Adda-Bedia, E. Katzav, and D. Vandembroucq, Phys. Rev. E **73**, 035106 (2006).
[36] J. W. Morrissey and J. R. Rice, J. Mech. Phys. Solids **46**, 467 (1998).
[37] I. Kolvin and M. Adda-Bedia (unpublished).
[38] M. Vasoya, A. B. Unni, J.-B. Leblond, V. Lazarus, and L. Ponson, J. Mech. Phys. Solids **89**, 211 (2016).
[39] See Supplemental Material at http://link.aps.org/supplemental/10.1103/PhysRevLett.119.215505 for details of the derivation of Eqs. (1) and (2), the explicit form of the crack front equation of motion to 2nd order accuracy, details of the numerical solution, a particular analytic solution for a time-independent cosine perturbation and a brief description of the supplementary movie files.
[40] E. Bouchbinder, A. Livne, and J. Fineberg, Phys. Rev. Lett. **101**, 264302 (2008).
[41] E. Bouchbinder, T. Goldman, and J. Fineberg, Rep. Prog. Phys. **77**, 046501 (2014).